World Journal of Microbiology and Biotechnology (2023) 39:187
https://doi.org/10.1007/s11274-023-03634-z

RESEARCH

Translational protein RpsE as an alternative target for novel nucleoside analogues to treat MDR *Enterobacter cloacae* ATCC 13047: network analysis and molecular dynamics study

Reetika Debroy[1,2] · **Sudha Ramaiah**[1,3]

Received: 22 February 2023 / Accepted: 26 April 2023 / Published online: 8 May 2023

Abstract
The pathogenic *Enterobacter cloacae* subsp. *cloacae* str. ATCC 13047 has contemporarily emerged as a multi-drug resistant strain. To formulate an effective treatment option, alternative therapeutic methods need to be explored. The present study focused on Gene Interaction Network study of 46 antimicrobial resistance genes to reveal the densely interconnecting and functional hub genes in *E. cloacae* ATCC 13047. The AMR genes were subjected to clustering, topological and functional enrichment analysis, revealing *rpsE* (RpsE), *acrA* (AcrA) and *arnT* (ArnT) as novel therapeutic drug targets for hindering drug resistance in the pathogenic strain. Network topology further indicated translational protein RpsE to be exploited as a promising drug-target candidate for which the structure was predicted, optimized and validated through molecular dynamics simulations (MDS). Absorption, distribution, metabolism and excretion screening recognized ZINC5441082 (*N*-Isopentyladenosine) (Lead_1) and ZINC1319816 (cyclopentyl-aminopurinyl-hydroxymethyl-oxolanediol) (Lead_2) as orally bioavailable compounds against RpsE. Molecular docking and MDS confirmed the binding efficacy and protein−ligand complex stability. Furthermore, binding free energy (G_{bind}) calculations, principal component and free energy landscape analyses affirmed the predicted nucleoside analogues against RpsE protein to be comprehensively examined as a potential treatment strategy against *E. cloacae* ATCC 13047.

Keywords Gene interaction network · Molecular docking · Molecular dynamics simulations · Binding free energy · Principal component analysis · Free energy landscape

Introduction

Genus *Enterobacter*, a group of serious human opportunistic pathogens, is associated with numerous nosocomial infections such as urinary tract infections, cholecystitis, osteomyelitis, and neonatal meningitis (Eugene Sanders and Sanders 1997). Most Enterobacter strains are documented to have acquired antimicrobial resistance (AMR), thus rendering their treatment strategy immensely complex and critical (Trivedi and Harish Shettigar 2015). *E. cloacae* subsp. *cloacae* str. ATCC 13047, a facultative anaerobic bacterium, displays multi-drug resistance (MDR) as revealed from antibacterial assays and whole genome sequencing, signifying the presence of multi-drug efflux systems, resistance to antimicrobial peptides and β-lactam resistance genes. Its complete genome consists of one circular chromosome of 5314.6 kb and two circular plasmids pECL_A and pECL_B of 200.4 kb and 85.6 kb respectively. Both the chromosome and plasmid are reported to encompass virulence genes involved in adhesion and invasion; moreover, the chromosome constitutes seven operon systems contributing towards toxic heavy metal resistance, as well as, numerous MDR genes that can play vital roles in bacterial pathogenesis (Ren et al. 2010). Due to its attained MDR, the strain received

✉ Sudha Ramaiah
sudhaanand@vit.ac.in

Reetika Debroy
reetika.debroy@vit.ac.in

[1] Medical and Biological Computing Laboratory, School of Bio-Sciences and Technology (SBST), Vellore Institute of Technology (VIT), Vellore, Tamil Nadu 632014, India

[2] Department of Bio-Medical Sciences, School of Bio-Sciences and Technology (SBST), Vellore Institute of Technology (VIT), Vellore, Tamil Nadu 632014, India

[3] Department of Bio-Sciences, School of Bio-Sciences and Technology (SBST), Vellore Institute of Technology (VIT), Vellore, Tamil Nadu 632014, India

massive attention among researchers to explore alternative therapeutic strategies to curb down its pathogenicity. The discovery of protein targets, which predominantly participate in MDR mechanisms in the strain, needs to be executed and the targets must be exclusively exploited to design specific leads for obstructing the resistance pathways (Shankar et al. 2021; Naha et al. 2021; Varghese et al. 2022). There have been existing reports of exploiting putative drug targets of pathogenic organisms for vaccine development to elicit a robust immune response against the associated infections. Immunoinformatics approach has been previously employed to construct multi-epitope vaccines against *Enterococcus faecium, Klebsiella pneumoniae, Pseudomonas aeruginosa, Acinetobacter baumannii* and many other complications (Narang et al. 2021, 2022; Dey et al. 2022a, b, c; Sudeshna Panda et al. 2022; Mahapatra et al. 2022a, b; Sahoo et al. 2022). However, the current research article has focused on identifying therapeutic lead molecules against *E. cloacae* and evaluating their interaction profile with potent drug targets. Computational studies have already been established to predict potential techniques and therapeutics in the field of medical research and diagnostic purposes (Sinha et al. 2019; Godara and Kao 2020; Sharma et al. 2021; Priyamvada et al. 2022; Kaviraj et al. 2022; Alam et al. 2023; Choudhary et al. 2023). Gene Interaction Network (GIN) approach integrated with structural bioinformatics can be useful in understanding the complex molecular interactions among the biomolecules present in the physiological systems (Naha et al. 2022; Priyamvada et al. 2022; Ashok and Ramaiah 2022). Our research group has previously decoded complex metabolic pathways and identified potent drug targets using network biology studies (Ashok et al. 2021, 2022; Naha and Ramaiah 2022), as well as integrated structural bioinformatics to predict effective lead molecules to circumvent several infectious and systemic diseases (Vasudevan et al. 2021; Miryala et al. 2021b; Debroy and Ramaiah 2022).

The present study was conducted to decipher the convoluted physiological processes and drug resistance mechanisms in *E. cloacae* str. ATCC 13047 using GIN studies. The genes directly (direct interactors) and indirectly (functional partners) involved in the biological pathways were categorized. Analyses of gene clusters, functional enrichment terms as well as network topological parameters were performed to strengthen our findings. This approach favorably led us to unravel the potential therapeutic markers that functionally interlinked vital metabolic processes in the bacteria. The highest scoring drug target based on GIN topological parameters was selected and its encoded protein structure was validated. Ligand-based virtual screening was performed to identify candidate molecules that can specifically bind with the target protein inhibiting its biomolecular activity (Swargiary et al. 2020). Molecular docking and molecular dynamics simulations (MDS) confirmed the binding efficacy and protein−ligand complex stability. Furthermore, binding free energy (G_{bind}) calculations, principal component (PC) and free energy landscape (FEL) analyses were performed to affirm the predicted drug candidates to be comprehensively examined for potential treatment strategy against the pathogen. This method can pave the path to a successful antimicrobial treatment strategy against the MDR strains of *E. cloacae*.

Methodology

GIN study

Data curation and retrieval of interaction data

Genes contributing to AMR in *E. cloacae* were obtained from the Pathosystems Resource Investigation Centre (PATRIC)v3.6.7 (http://www.patricbrc.org) database (Wattam et al. 2014). Information regarding various biological interactions including the experimental validated and computationally predicted interactions among the provided genes were gathered from the Search tool for the retrieval of interacting genes and proteins (STRING)v11.0 (https://string-db.org/) database (Szklarczyk et al. 2017). STRING assigned a confidence score (CS) to each interaction based on experimental and prediction data available (Mering 2003). High CS value indicated the data to be more reliable and reproducible.

Functional enrichment analysis (FEA), GIN visualization and analysis

The STRING database provided various functional enrichment terms from KEGG pathways, UniProt terms, Pfam, InterPro and SMART domains. The resultant GIN was visualized in Cytoscape v3.7.2 (http://www.cytoscape.org/) to comprehensively display the genes and their associations (Shannon et al. 2003). Gene clustering was performed byMCODEv1.5.1, a Cytoscape in-built tool, which utilized the functional enrichments of each gene and performed clustering based on their functional associations. It assigned a score to each cluster based on the density and the number of members in a particular cluster (Bader and Hogue 2003). NetworkAnalyzer v2.7, another Cytoscape plug-in, estimated the network topological matrices to simplify the complex biological networks and provide us with intrinsic details regarding each gene (Fiannaca et al. 2013).

Protein structure prediction, refinement and validation

The top-ranked hub gene attaining the highest clustering and topological coefficients, along with functional relevance in the network was selected and the structure of its encoded

protein was predicted. In case the structure was unavailable in the Protein Data Bank (PDB) (https://www.rcsb.org/), the 3D structure of the protein was modeled as per the 'extended dual-step modeling method' as proposed by Basu et al. (2021) to minimize the local conformational errors thus enhancing the gross accuracy of the model (Shankar et al. 2021; Basu et al. 2021; Naha et al. 2022). The generation of the 3D model was based on homology (template-based) modeling and threading with I-TASSER (https://zhanglab.ccmb.med.umich.edu/I-TASSER/), RaptorX (http://raptorx.uchicago.edu/), and Robetta (https://robetta.bakerlab.org/) servers (Kim et al. 2004; Yang and Zhang 2015; Wang et al. 2016). Based on high C-score denoting the models' global accuracy, low estimated RMSD and low local error estimates, the top ranked model from each server was selected as a template to model the final 3D structure using MODELLER 10.0, a python-based standalone software with modeling method analogous to NMR spectroscopy-based structure illustration (Webb and Sali 2017). The structure was refined through GalaxyRefine (http://galaxy.seoklab.org/index.html) web server to reduce the clash scores, poor rotamers and Ramachandran outliers (Heo et al. 2013). Energy minimization was performed *in vacuo* with GROMOS96 43B1 force-field mechanics in Swiss-PDB viewer v4.1.0 (Kaplan and Littlejohn 2001). The optimized protein structure was visualized in USCF Chimera v1.9 (Pettersen et al. 2004). The secondary structure prediction of the refined protein was performed by SOPMA (https://npsa-prabi.ibcp.fr/cgi-bin/npsa_automat.pl?page=npsa_sopma.html) (Geourjon and Deléage 1995) and PSIPRED (http://bioinf.cs.ucl.ac.uk/psipred/) servers (McGuffin et al. 2000), whereas, the tertiary structure was validated through HARMONY (http://caps.ncbs.res.in/harmony/) (Pugalenthi et al. 2006) and ProSAWeb (https://prosa.services.came.sbg.ac.at/prosa.php) servers (Wiederstein and Sippl 2007). Protein backbone dynamics at the residue level were predicted in terms of N–H S^2 bond-order restraints using DynaMine (http://dynamine.ibsquare.be/) server to study the restriction in the movement of an atomic bond vector with respect to the molecular reference frame (Cilia et al. 2014). ProtParam (https://web.expasy.org/protparam/) server was used to compute parameters such as amino acid composition, aliphatic index (for thermo-stability and structural rigidity measure) and instability index of the protein (Gasteiger et al. 2005).

Analysis of protein stability through molecular dynamics simulations (MDS)

MDS was performed using GROMACS 2018.1 package to analyze the protein stability in an aqueous environment over a time frame of 100,000ps. Protein topology was generated using CHARMM36 (February 2021) force field mechanics. Solvation was performed by centering the protein inside a cubic box (1.0 nm) with a simple-point charge water model, followed by system neutralization upon the addition of requisite counter ions (Na^+ or Cl^-) using the particle mesh Ewald method. Energy minimization was carried out using steepest descents method with 50,000 steps and potential energy gradient threshold of 1000 kJ/mol/nm. System equilibration was performed under NVT (Number of particles, Volume, Temperature) (desired temperature = 300 K) and NPT (Number of particles, Pressure, Temperature) (desired pressure = 1 bar) ensembles for 100ps utilizing Parrinello–Rahman proposed barostat method, followed by unbiased MD production to provide the trajectory data. Root mean-square deviation (RMSD) analysis of the simulated protein reflected the net change (in nm) in the backbone configuration, while root mean-square fluctuation (RMSF) per residue denoted the average fluctuation (in nm) of each amino acid residue present in the protein. The stability of the folded protein structure was interpreted from radius of gyration (Rg) trajectory over the stipulated time period estimating the compactness of the structure, while potential energy trajectory depicted the stability of the energy parameters of the stimulated system (Hamelberg et al. 2004; Jayaraman et al. 2019; Lemkul 2019; Basu et al. 2021; Miryala et al. 2021b).

Protein druggability analysis, virtual and pharmacokinetic screening of ligands

DoGSiteScorer (http://dogsite.zbh.uni-hamburg.de) server was used to predict potential binding pockets in the protein (by surface topology scan) and subsequently computed the druggability of these pockets (Volkamer et al. 2012). An established inhibitory compound against potential target was selected as a reference to screen analogous ZINC drug-like compounds. This ligand-based virtual screening was performed with SwissSimilarity (http://www.swisssimilarity.ch) server (Zoete et al. 2016). The top ranked analogues were further selected for pharmacokinetic and ADME screening through SwissADME (http://www.swissadme.ch/) server (Daina et al. 2017).

Site-specific molecular docking

The ligand analogues selected after ADME screening were firstly subjected to energy minimization through the auto-optimization function of the Avogadro tool using Universal force-field and steepest descent algorithm (Hanwell et al. 2012). The optimized ligands were considered for molecular docking with the active site (functional domain) of the drug target using AutoDock v1.5.6 suite. Protein structures were firstly optimized by adding polar hydrogen (H–) atoms and merging non-polar atoms, followed by addition of requisite Kollman charges. The affinity grid-boxes ($60 \times 60 \times 60$ $Å^3$) were created encompassing the active-site residues of

proteins. Lastly, Lamarckian and Genetic Algorithms were utilized to generate probable protein−ligand complex conformations (Basu et al. 2022a, b). Protein−ligand docked poses and their intermolecular interactions were visualized in Discovery Studio Visualizer v2020. Moreover, comparative molecular docking of the drug-target with a standard antibiotic (with reported inhibition profile against the drug-target) was further performed to provide a quantitative measure of docking efficacy between the novel lead and the protein (Debroy and Ramaiah 2022).

Analysis of protein−ligand stability through MDS

The stability of drug-target-ligand/lead complexes was performed in an aqueous environment for a time-frame of 100,000ps using GROMACS 2020.2 package. Protein topology was built as described previously (in "Analysis of protein stability through MDS" section), whereas ligand topology was built using the CGenFF server. The complex was centered inside a dodecahedron box of uniform edge-distance (1.0nm) followed by solvation with a simple point-charge water model and system neutralization with requisite counter ions (Na^+ or Cl^-). Steepest-descents algorithm (50,000 steps) and convergence-tolerance force (1000 kJ/mol/nm) were considered for the system-energy minimization. Two cycles of equilibrations were opted with constant volume (NVT) ensemble for 100ps using leap-frog integrator to attain the desired temperature (300 K). Secondly, constant pressure (NPT) ensemble for 100ps using the Parrinello–Rahman barostat was applied to attain desired pressure (1 bar) upon applying motion-equations to the box vectors. Long-range electrostatic interactions were treated using particle-mesh Ewald algorithm with a cubic interpolation of order 4.0 and Fourier spacing of 0.16 nm (Jayaraman et al. 2021). Finally, the system was subjected to MD production for 100,000ps timescale (Lemkul 2019; Miryala et al. 2021b; Naha et al. 2022).

Protein−ligand binding free-energy calculations and principal component (PC) based free-energy landscape (FEL)

Interaction energy (IE) or linear interaction energy calculations have been depicted as an efficient approach to scale absolute binding free energy (G_{bind}) between a protein and ligand. According to simulations of the ligand's protein-bound and unbound states in a solvent, G_{bind} is postulated in IE to be linearly proportional to the variations in van der Waals and electrostatic interactions involving the ligand and its surroundings (or bound protein). The free-energy differences were modeled considering short-range/long-range electrostatic IE parameters using Lennard-Jones (LJ) and Coulomb potential-energy functions (Rifai et al. 2019). The IE was calculated through a 10 ns timescale re-run, using similar pressure-coupling and electrostatic considerations as performed during simulation by GROMACS 2020.2 package.

The biological functionality of a protein is heavily influenced by its molecular motions. PCA or essential dynamics is employed to extract and investigate high collective motions from a structural ensemble using covariance matrices. PCA lowers the dimensionality of MDS trajectory data required to describe protein dynamics. The atomic coordinates procured from protein alpha-carbon (Cα) atoms were utilized for covariance matrix construction due to its depiction of essential space motions and less interference by statistical noise. The collective motions of the biological systems were stored as eigenvectors and eigenvalues representing the direction of concerted motion and magnitude in the direction of motion respectively. The first few eigenvectors are referred to as PCs that capture the highest eigenvalues (Kumar et al. 2020). The cosine content value of PCs is employed to extract the strenuous motion from the overall collective motions, and it ranges from 0 (no cosine) to 1 (perfect cosine) for a time period of T:

$$C_{\mathrm{i}} = \frac{2}{\mathrm{T}}\left\{\int \cos 2(i\pi t)p_i(t)dt\right\}^2\left(\int p_i^2(t)dt\right)^{-1}$$

Generally, the top eigenvectors having cosine content values lower than 0.2 were utilized to interpret the conformational space and protein dynamics in terms of FEL. Accordingly, the first ten projections were retrieved and their cosine content values were calculated. The minimized structures obtained from the FEL plot represent the lowest energy-stable state of that protein. The GROMACS in-built tools such as 'gmx covar' and 'gmx anaeig' are employed to construct the covariance matrix and the projections of trajectories onto the eigenvectors respectively. Furthermore, 'g_sham' module was employed to generate smooth FEL plots of the protein−ligand complexes (Jayaraman et al. 2021). The 'g_sham' script was utilized to map all the probable protein confirmations by means of Gibb's free energy through Mathematica tool. Using two-dimensional (2D) and three-dimensional (3D) FEL plots, two PCs (PC1 and PC2) of the different protein−ligand complexes were projected (Swetha et al. 2017; Jayaraman et al. 2019). Furthermore, the overall conformational change in the protein structure was estimated through RMSD calculations (in Å) with respect to C-α backbone using Swiss-PDB viewer v4.1.0.

RESULTS

Collection of AMR genes and retrieval of interaction profile

Sixty-seven AMR genes from *E. cloacae* were filtered out of 107 genes to avoid redundancies. Subsequently, the

interaction profile of 46 nodes (genes) having 378 edges (interactions) was extracted encompassing data from experimentally evident analysis, computational predictions and literary evidence. This approach enabled us to amalgamate established as well as novel molecular pathways/markers, which might facilitate a better understanding of alternative treatment strategies. The AMR genes with their corresponding functional partners and their respective CSs are provided in Supplementary File S1.

FEA, gene clustering and network topology analysis

Five KEGG pathways, 17 UniProt keywords, nine Pfam domains, 20 InterPro domains and three SMART domains were collected for 46 AMR genes. The descriptions of the enrichment terms along with the genes corresponding to each term are detailed in Supplementary File S2. MCODE clustered 34 out of 46 genes into three gene clusters, i.e., C1, C2 and C3, ranked based on decreasing MCODE scores. Clusters C1, C2, C3 consisted of 19, 12, 3 nodes and 162, 40, 3 edges with MCODE scores of 18.000, 7.273, 3.000 respectively, as displayed in Fig. 1 a. The complete network, as well as discrete genes, were analyzed based on several topological parameters, which are tabularized in Supplementary File S3.

Genes in C1 cluster

C1 had an average clustering coefficient value of 0.73, implying dense interconnections among the clustered genes. Genes *rplF* and *rplR* encode for 50S ribosomal large subunit proteins L6 and L18 respectively; whereas *rpsC, E, G, H, J, L* encode for 30S ribosomal small subunit proteins S3, S5, S7, S8, S10 and S12 respectively (ecln03010; KW-0689). From the gene network, we noted that *rplF* made interactions of high confidence with *rplR, rpsE, rpoB,C* (ecln03020; KW-0240), *fusA*(*ECL_01886*), *ileS* and *gyrA*. The gene *rplR*, similar to *rplF* made high confidence associations with *rpsE, fusA, rpoB*, and *rpoC*. The *rps* gene family displayed high confidence interactions among its members, as well as with *rplF,R*, *rpoB,C* and *fusA*. The genes *rpsC,E*, absent in the first STRING set, were linked with *gyrA*, unlike other *rps* genes. The genes *gyrA* and *parC* were the most interacting genes in the entire network having the top degree values of 33 and 31 respectively. *gyrA* made a notable high confidence association with *ampC* (*ECL_00553*) from C2 signifying its association with the cephalosporinase gene. Likewise, *gyrB* and *parE* (PF00986; IPR013759; SM00433) acquired high degree values of 31 and 30 respectively. It was eventually observed that gene *rpsE*, encoding for 30S ribosomal subunit protein S5, made direct and indirect links with ribosomal large subunit proteins, RNA polymerase subunit proteins, elongation factor G, DNA gyrase and DNA topoisomerase IV subunit proteins, as displayed in Fig. 1b. Hence RpsE, being an integral component in bacterial machinery and the interaction network, can be considered to be a candidate for being a potential drug target.

Genes in C2 cluster

The clustering coefficient of C2 was recorded to be 0.68 implying the interconnections were quite as dense as that observed in the C1 cluster. The genes *macB* and *msbA* (*ECL_01832*) were enriched with similar annotations making dense interconnections. In the current study, *macB* made high confidence interaction with *acrA* (C3); moreover, *msbA* did not make any such association with other genes. However, neither of the two genes interacted with the other in the gene network. The gene *murA* (MurA) gave a degree value of 24, making it the most interacting gene of C2 cluster. Despite its high number of interactions, *murA* made only one interaction at high confidence with *glpT*. The genes *acrB, oqxB* and *mdtC* were annotated with similar enrichment terms. AcrB is a major component of the AcrAB-TolC system in several MDR Gram negative bacteria (ecln01501; ecln01503; PF00873; IPR027463). GIN analysis revealed that *macB*, *mdtC* and *oqxB* established direct interactions with *acrA* (Fig. 1b). *acrA*, being the common functional partner, connected the entire MDR efflux network, thus signifying its pivotal role as a hub gene. Therefore, AcrA can be considered a candidate drug target in *E. cloacae* str. ATCC 13047.

Genes in C3 cluster

The average clustering coefficient of C3 was computed to be 0.62 indicating quite dense interconnections among the three nodes. The C3 genes *arnA, C*, along with unclustered gene *arnB*, were enriched with similar annotations (ecln01503; KW-0441). In the present study, GIN revealed *arnT* as the interlinking biomolecule associating all other *arn* genes (Fig. 1b). Hence, ArnT protein can be a candidate drug target for subduing CAMP resistance.

Out of the three proposed drug targets, as displayed in Fig. 2, *rpsE* procured the highest degree, highest MCODE score and highest clustering coefficient, making the overall topological coefficient higher than *acrA* and *arnT* as represented in Supplementary File S3. Hence, RpsE was selected for further structural analysis and can be checked for being a potential drug target against the pathogenic strain.

Structure prediction, refinement and validation of RpsE protein

The unavailability of crystal structure for RpsE from *E. cloacae* ATCC 13047 according to PDB search using

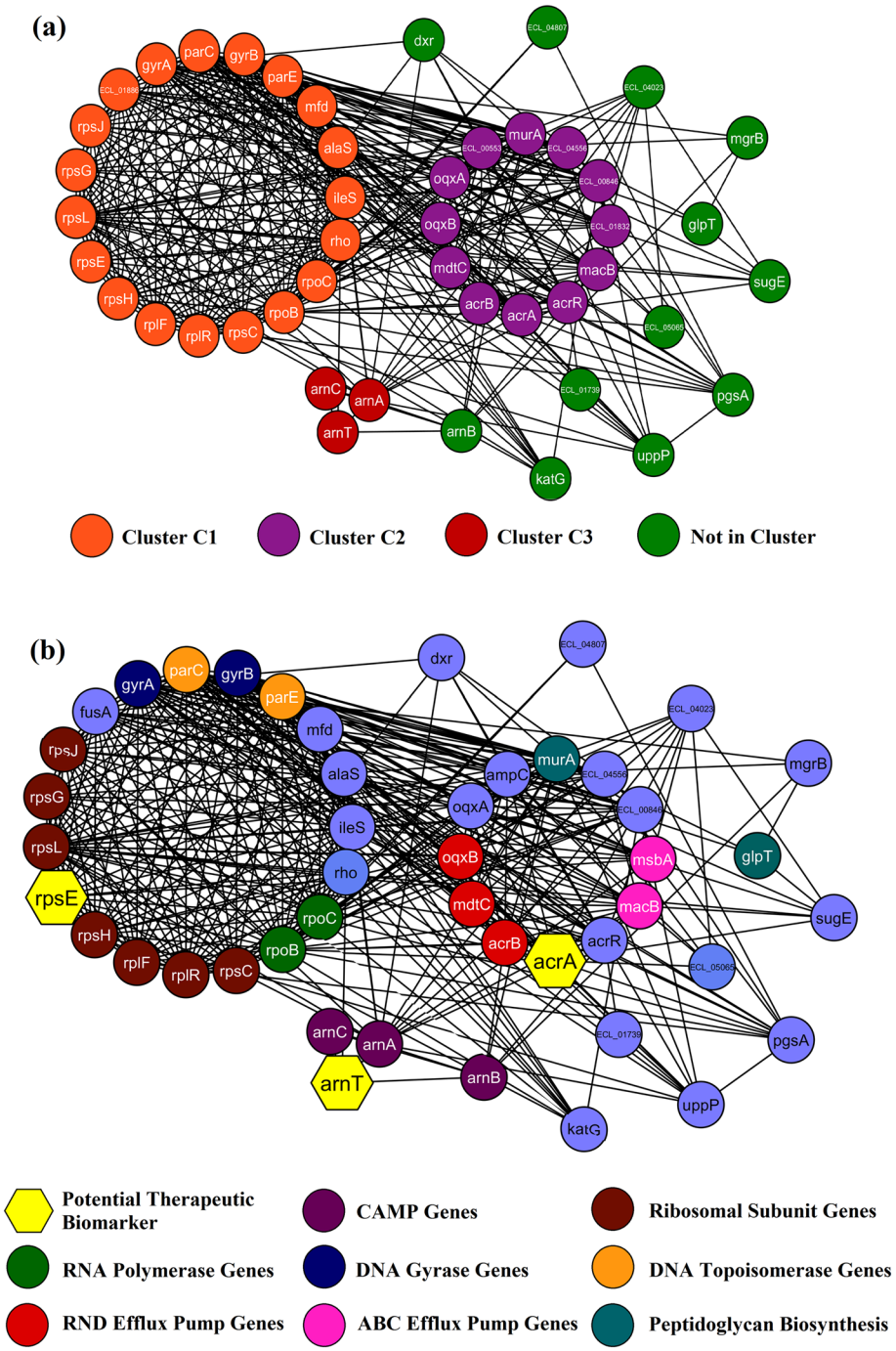

Fig. 1 GIN analysis of AMR genes in *E. cloacae* ATCC 13047: **a** AMR gene clustering resulted in three clusters-C1, C2, C3 based on the functional associations of the genes, **b** FEA of AMR genes highlighted the enriched pathways, as well as predicted therapeutic drug targets based on the pathway enrichment and interaction patterns

NCBI-BLASTp tool prompted for the 'extended dual-step modeling method'. RpsE 3D structure prediction was performed from *E. cloacae* ATCC 13047 protein sequence (UniProt ID: A0A0H3CSH0). The 3D modelled RpsE protein (Fig. 3a) was optimized and refined, which eventuated the model to be comprised of 100.0% residues in Ramachandran favored zone with low RMSD (0.298 Å) and the absence of any poor rotamers. The refined protein laid close to the straight fit line of the HARMONY propensity-calibration plot (Fig. 3b), as well as displayed minimal regions of reverse sequence acquiring better substitution scores than query sequence (Fig. 3c). The protein acquired ProSAWeb Z-score (indicating overall model quality) of − 6.38 and fell within the score-range of NMR determined (experimentally established) native structures (Fig. 3d). The protein acquired an overall negative value in the energy plot for local model quality (Fig. 3e). The above quality analyses validated low misfold regions, low local errors, absence of erroneous regions and a highly restricted backbone of structurally improved RpsE model. RpsE from *E. cloacae* ATCC 13047

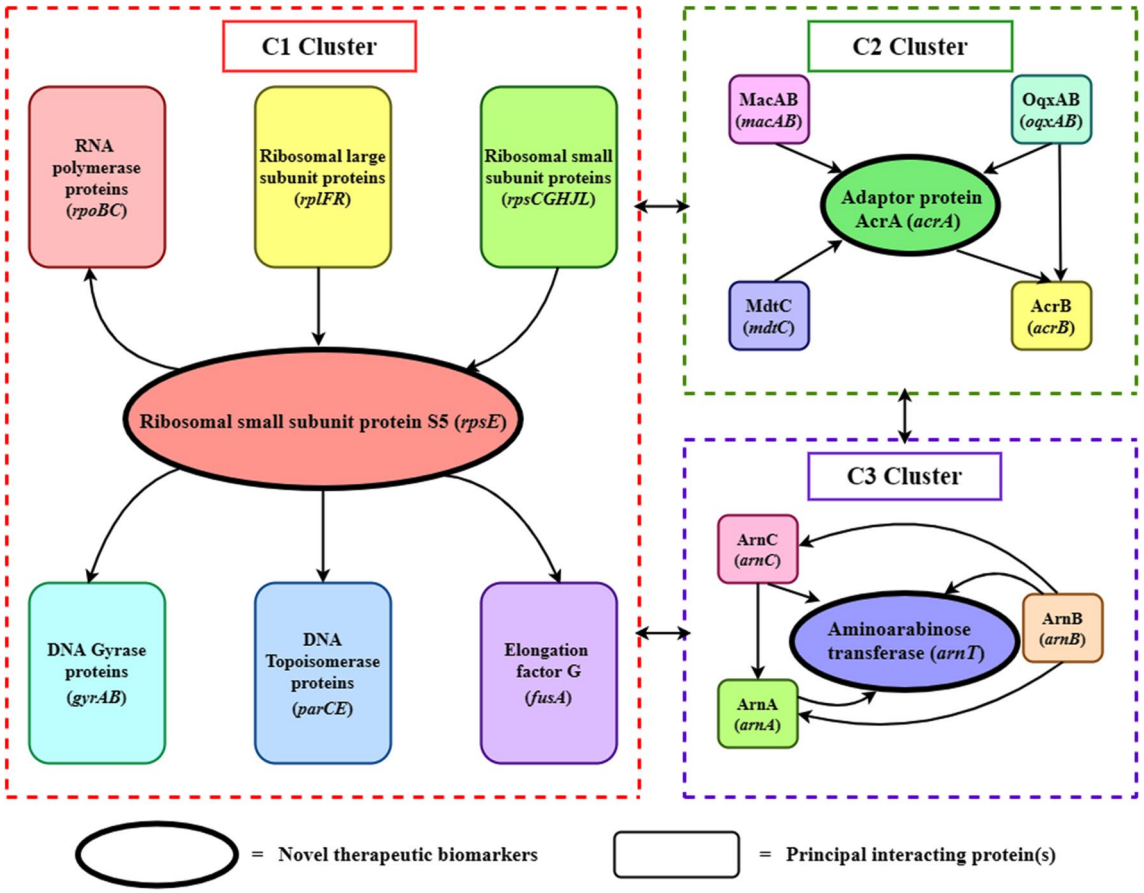

Fig. 2 Identification of novel therapeutic drug targets in MDR strain *E.cloacae*ATCC 13047: the proposed novel therapeutic markers, 30S ribosomal subunit S5, AcrA and ArnT proteins along with their principal interacting protein(s) are displayed. The major functional pathways enriched in each cluster have been highlighted, which showed C1 cluster containing general metabolism-linked genes while C2 and C3 genes involved in AMR mechanisms

constitutes an RNA-binding region [PROSITE ID: PS50881] from the 11th to 74th amino acid residue in the *N*-terminal domain [InterPro ID: IPR013810; Pfam ID: PF00333] of the protein. Secondary structure prediction revealed that the RNA-binding domain of RpsE protein resided in the cytoplasm consisting of α-helices (42.2%), extended strands (32.8%), random coils (12.5%) and β-turns (10.9%). While predicting the residue-level backbone dynamics, the RNA-binding region acquired an average N–H S^2_{pred} value of 0.82 (Fig. 3f). RpsE attained an aliphatic index of 89.88 implying high thermo-stability and a well-packed protein interior (high structural rigidity). The instability index of RpsE was computed to be 32.72, further implying the protein stability.

RpsE stability analysis through MDS

The stability of RpsE protein in an aqueous environment was analyzed over a time-frame of 100 ns. The RMSD trajectory was maintained at around 0.6 nm throughout the timescale, as shown in Fig. 4a, suggesting minimal mean deviations indicating protein stability. RMSF plot depicted low residue-level positional dynamicity (< 0.4 nm) of the functional domain; however, a meager peak was recorded within the 22nd–33rd amino acid residues, as displayed in Fig. 4b. The stable protein conformation was validated by the consistent Rg (fluctuating within 1.7–1.8 nm) trajectory throughout the time frame, as seen in Fig. 4c, implying the compactness and well-folded conformation of RpsE. The potential energy curve displayed average stability at − 1.2958e + 06 kJ/mol, as shown in Fig. 4d validating the energy functions supporting the simulated system. The temperature of the system quickly reached the target value (300 K) and remained stable over the remainder of the equilibration (Supplementary File S4a), while the average value of pressure was computed to be 1.5 bar which was close to the desired value (1 bar) (Supplementary File S4b), thus indicating that 100ps of NVT and NPT were sufficient to equilibrate the system.

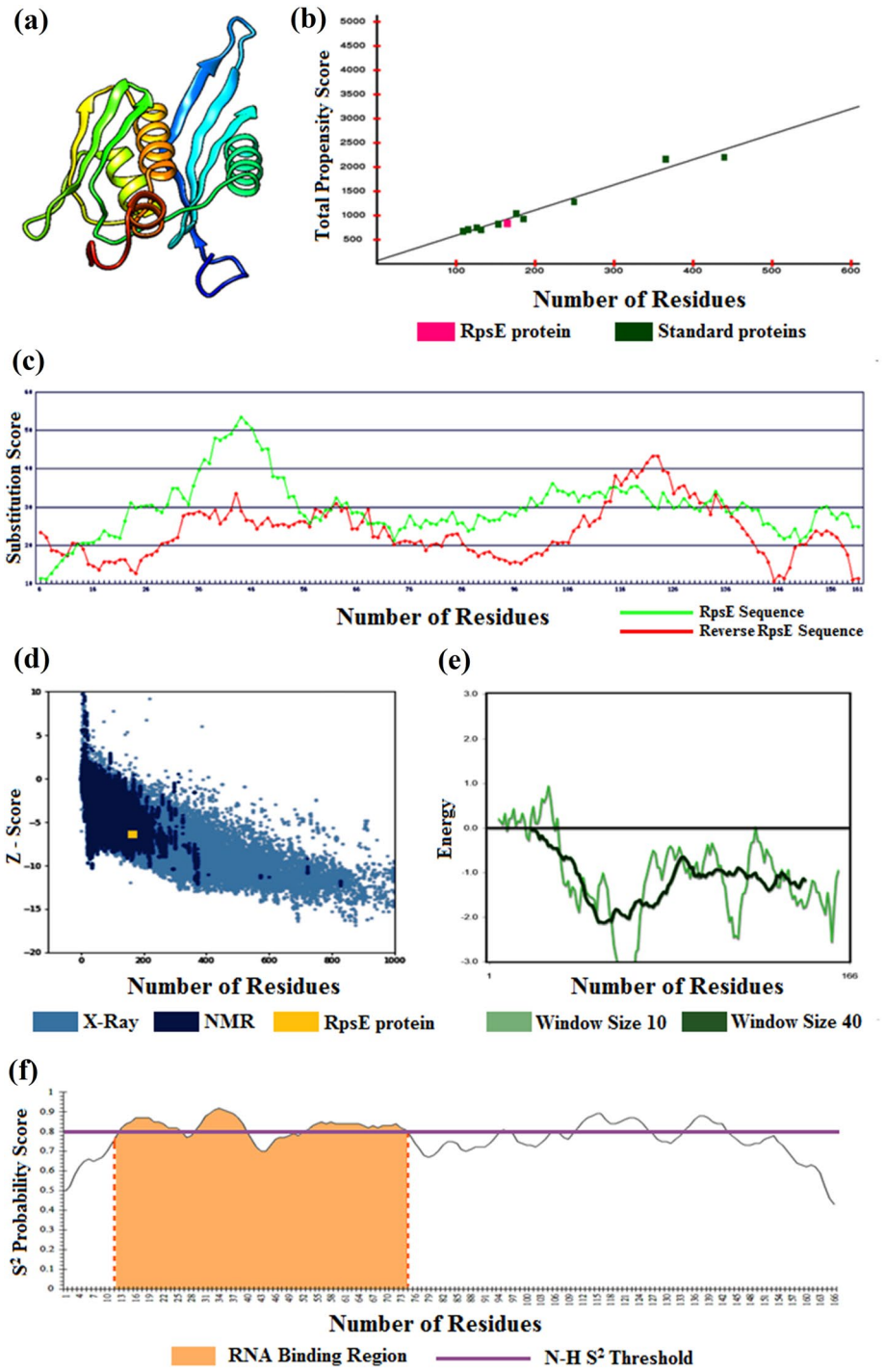

Fig. 3 Structural evaluation and validation of RpsE protein: **a** optimized modelled RpsE structure as visualized in USCF Chimera v1.9, **b** propensity plot of RpsE indicating low regions of misfolds, **c** substitution curve of RpsE implying absence of erroneous regions, **d** global model quality of RpsE displaying low overall structural errors, **e** local model quality of RpsE showing low local errors, **f** backbone stability plot of RpsE indicating highly restricted backbone of RpsE model

Protein druggability analysis, virtual and pharmacokinetic screening of ligands

A binding pocket overlapping with RNA binding domain was predicted, which attained a high drug score (0.85) and simple score (0.52) implying high druggability of the pocket further indicating that the protein can be a candidate for a potential therapeutic drug target. Ligand-based virtual screening was performed considering 2-methylthio-n6-isopentenyl-adenosine-5′-monophosphate (DB08185) as the reference molecule due to its reported inhibition activity against 30S ribosomal subunit proteins. Screening ZINC drug-like molecules against reference compound provided a list of similar hits, ranked based on descending Tanimoto coefficients (Zoete et al. 2016). The top 10 analogues with the highest Tanimoto scores, provided in Supplementary File

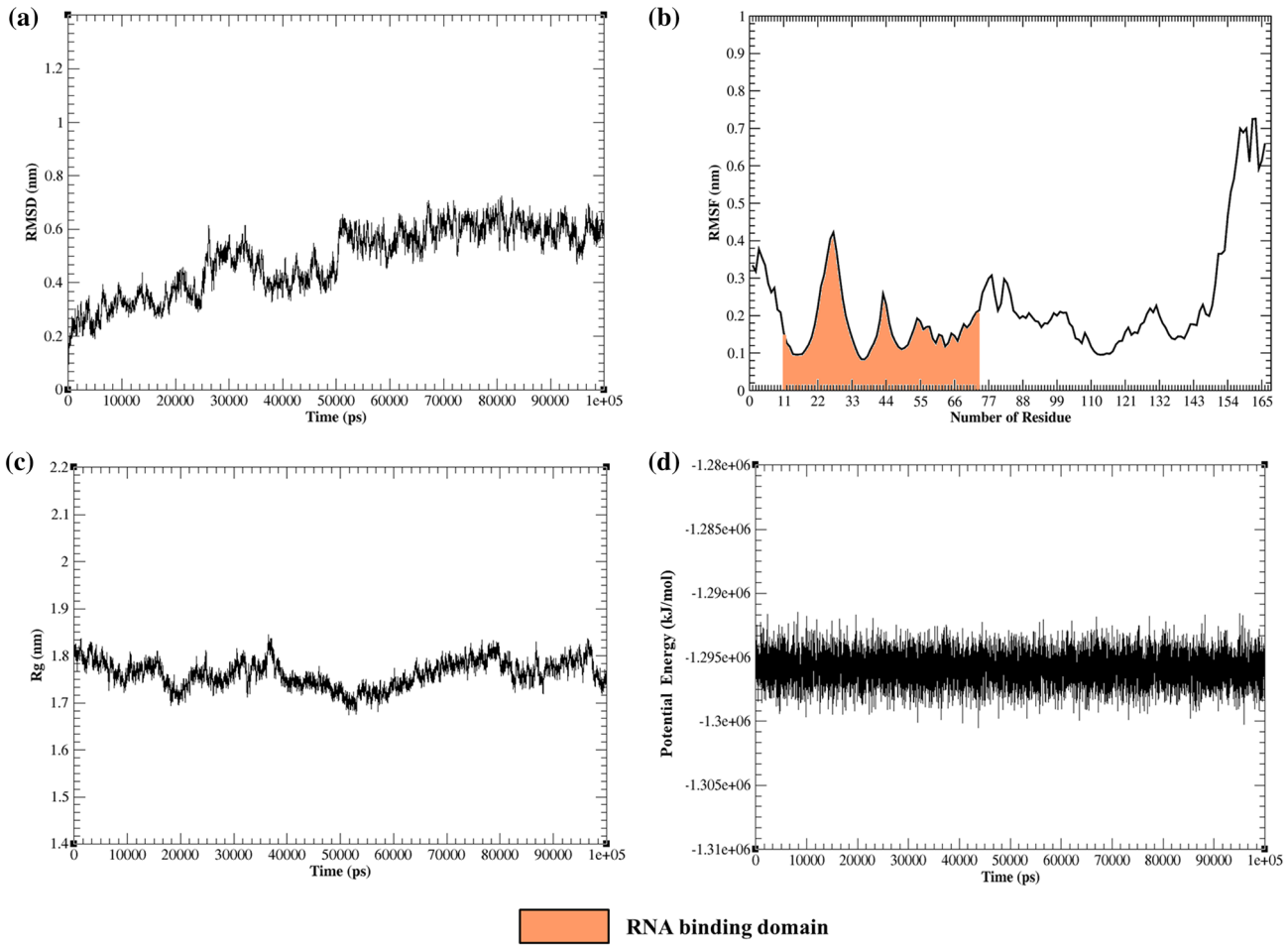

Fig. 4 Stability analysis of RpsE protein using molecular dynamics simulation (MDS): **a** RMSD plot of RpsE suggesting minimal mean deviations, **b** residue-level RMSF plot of RpsE depicting low residue-level positional dynamicity in the functional domain, **c** Rg trajectory of RpsE showing compact conformation of protein, **d** potential energy curve of RpsE validating the energy functions supporting the protein system

S5, were selected for further pharmacokinetic and ADME screening. Out of 10 compounds, ZINC5441082 (referred to as 'Lead_1' in the current study) and ZINC1319816 (referred to as 'Lead_2') fell within the bioavailability radar for drug-likeliness measure and were predicted to be orally bioavailable. The compounds successfully passed Lipinski's filter for ADME screening, displayed a high possibility of passive absorption by the gastrointestinal tract and were computed to be highly water soluble. Hence, ADME screening predicted the two commercially available compounds to be oral drug candidates against RpsE protein.

Assessment of intermolecular interactions of lead compounds with active-site of RpsE

The 'RpsE-inhibitor' docked complexes were generated by considering Ile30 as the active site for being a crucial residue in Spectinomycin (standard antibiotic) binding (Bollen et al. 1969; He et al. 2005; Dharuman et al. 2021). Lead_1 and Lead_2 were bound to RpsE with BEs of $-5.06 \pm 0.06$and -4.48 ± 0.30 kcal/mol with average inhibition constant (IC) of 0.20 and 0.56 mM respectively. The values were distinctly lower than Spectinomycin [PubChem CID: 15,541], with BE of -4.26 ± 0.37 kcal/mol and an average IC of 0.86 mM. It was inferred from the computed values that Lead_1 and Lead_2 required less energy to bind with RpsE as compared to its standard antibiotic Spectinomycin; moreover, lower IC values of the leads implied that lower concentrations are required by Lead_1 and Lead_2 to inhibit the RNA-binding activity of RpsE than that required by Spectinomycin. A comparable number of total intermolecular interactions (with respect to leads) were recorded between Spectinomycin and RpsE-active site namely six conventional H-bonds, one van der Waals interaction and two carbon–hydrogen (C–H) bonds as displayed in Fig. 5a. Lead_1 when complexed with RpsE formed three H-bonds, one van der Waals interaction,

two carbon–hydrogen (C–H) bonds and three non-canonical bonds (Fig. 5b). Meanwhile, Lead_2 formed three H-bonds, one van der Waals interaction, one carbon–hydrogen (C–H) bond and three non-canonical bonds with RpsE-active site (Fig. 5c). Despite high BE, higher number of conventional H-bonds and a lower number of non-canonical interactions were noted in RpsE_Spectinomycin complex compared to the other two complexes.

'RpsE-inhibitor' complex stability

Over the time frame of 100 ns, the RMSD trajectory of RpsE-Spectinomycin complex was stabilized at around 0.7 nm, whereas RpsE-Lead_1 and RpsE-Lead_2 complexes were stabilized at around 0.5 and 0.6 nm respectively (Fig. 6a). Low overall residue-level positional dynamicity (< 0.5 nm) of the RNA-binding domain was observed for all the complexes in the RMSF plot, however distinct fluctuations were recorded within 21st–30th amino residues, as displayed in Fig. 6b. The structural compactness of the protein−ligand complexes was validated by the stable Rg trajectory (consistent within the range of 1.7–1.8 nm) throughout the time frame (Fig. 6c). The SASA plot revealed similar convergence of the three complexes (at 100–105nm^2) throughout the timescale (Fig. 6d), whereas similar trajectory convergence of free energy of solvation for the three

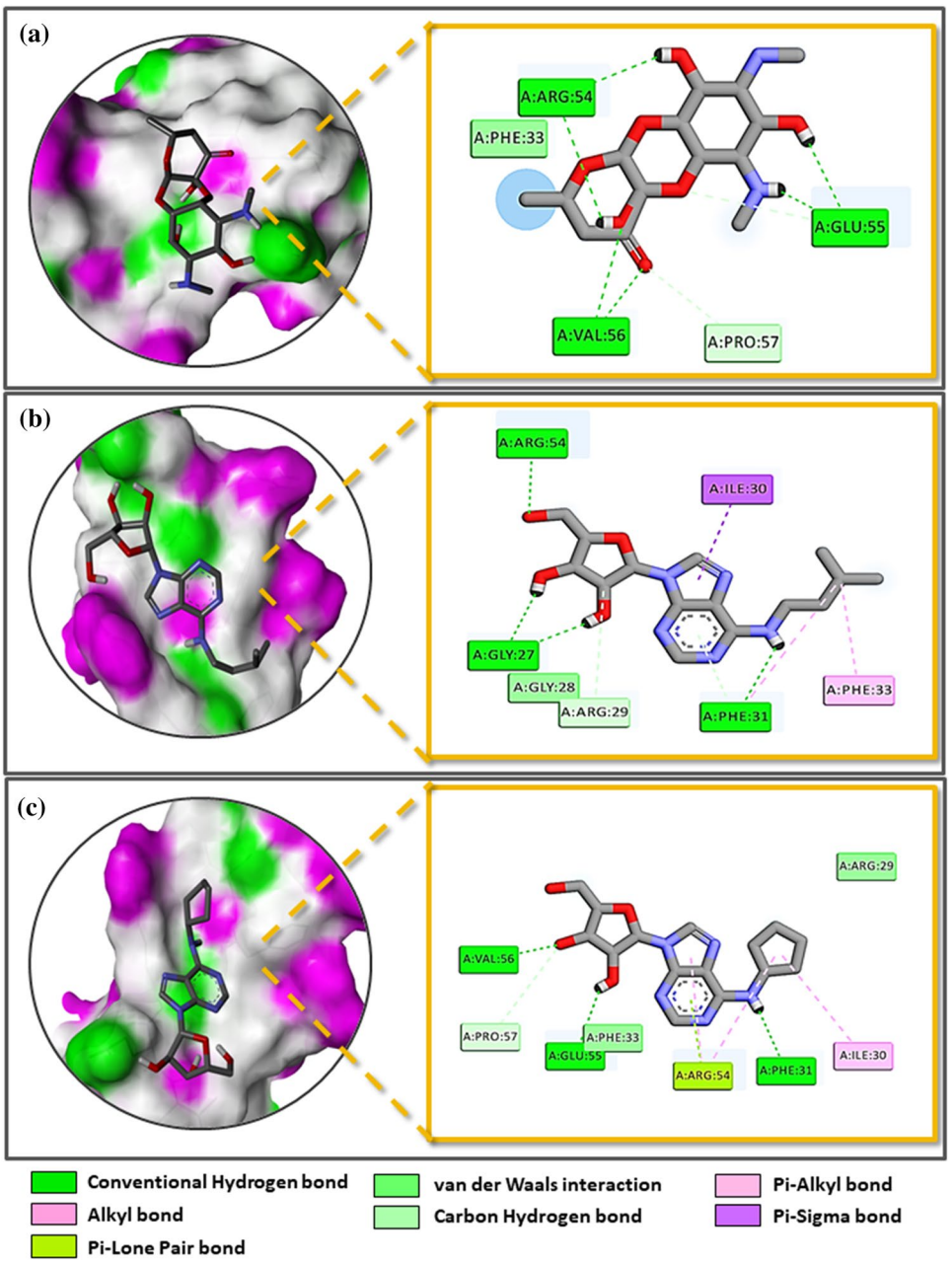

Fig. 5 Molecular docking of spectinomycin and lead compounds with RpsE: the docked poses and intermolecular interactions of spectinomycin and lead compounds with RpsE-active site are shown. **a** Docked pose and intermolecular interaction profile of RpsE-spectinomycin complex, **b** docked pose and intermolecular interaction profile of RpsE-Lead_1 complex, **c** docked pose and intermolecular interaction profile of RpsE- Lead_1 complex

complexes (~ − 27 to − 15 kJ/mol) was observed, indicating them to be comparably energetically favorable (Fig. 6e). The interaction energy implied energetically stable (< 0 kJ/mol) profiles for RpsE-Spectinomycin, RpsE-Lead_1 and RpsE-Lead_2 complexes (Fig. 6f). The temperature plots of the complex systems quickly reached the target value (300 K) and remained stable over the remainder of the equilibration (Supplementary File S6a,c,e). The pressure values, however fluctuated widely throughout the 100ps equilibration phase (Supplementary File S6b,d,f). The average pressure values of RpsE-Lead_1, RpsE-Lead_2 and RpsE-Spectinomycin complexes were computed to be − 15.86 bar, − 20.36 bar and − 20.61 bar respectively. Pressure can fluctuate widely throughout an MD simulation with a wide range of

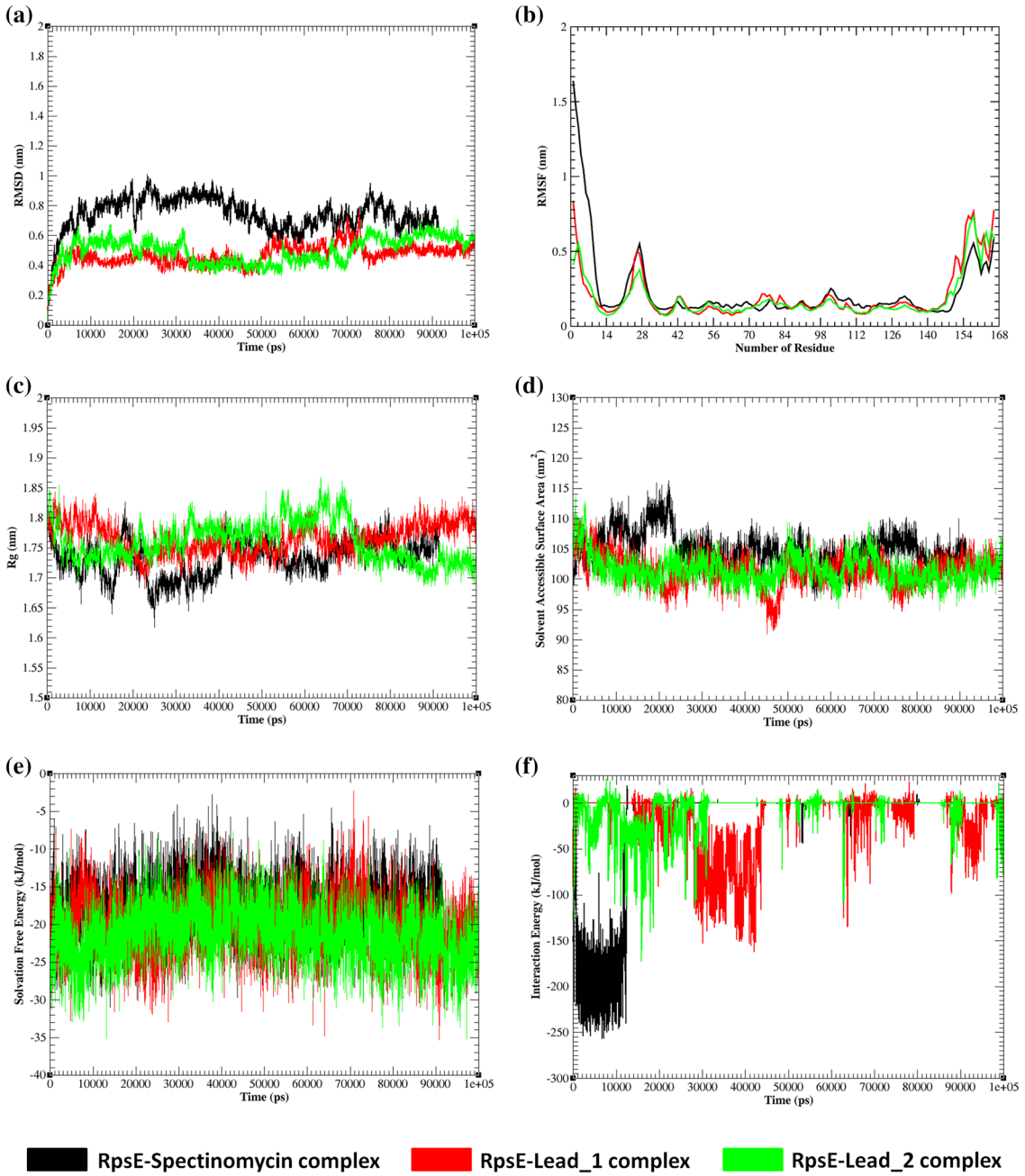

Fig. 6 Stability analysis of RpsE-lead molecules complexes as compared to RpsE-spectinomycin complex using MDS: **a** RMSD plot showing stabilized trajectories, **b** residue-level RMSF plot depicting low overall residue-level positional dynamicity of the RNA-binding domain, **c** Rg trajectory showing structural compactness of the protein−ligand complexes, **d** SASA trajectory revealed similar convergence of the three complexes throughout the time-scale, **e** free energy of solvation revealed similar trajectory convergence for the three complexes, **f** interaction energy implied energetically stable profiles for all the complexes number of hydrogen bonds in the complexes

root-mean-square fluctuations (in bar); hence, statistically difference between the obtained average and the target/reference value (1 bar) cannot be distinguished (Lemkul 2019). Thus, the plots indicated that 100ps of NVT and NPT were sufficient to equilibrate the protein-inhibitor complex systems. The intermolecular H-bond patterns showed that out of six probable H-bonds (from molecular docking), RpsE-Spectinomycin complex showed a maximum of four stable H-bonds in the time-frame of 100 ns, whereas RpsE-Lead_1 and RpsE-Lead_2 have displayed five and three stable H-bonds respectively, the latter correlating with the docking results (Fig. 7a–c).

Gibb's free energy calculations and FEL analyses

PC-based FEL analysis depicted the correlation differences among the three complexes. Motional shifts across two PCs (PC1 and PC2) were considered to define dynamic behavior and fluctuation degrees within the protein systems. The different ensemble of confirmations of the population basins at variable widths on the FEL plot defined the different equilibrium states of the protein. The RpsE-Spectinomycin {Gibbs free energy (G) range = 0–11.8 kJ/mol}, RpsE-Lead_1 (G-range = 0–10 .9 kJ/mol) and RpsE-Lead_2 (G-range = 0 – 0.9 kJ/mol) complexes exhibited distinct energy clusters. The low energy (low G) cluster basins were distinct among the three complexes. The RpsE-Lead_1 (Fig. 8b) and RpsE-Lead_2 (Fig. 8c) complexes showed three distinct 'lowest free energy cluster basins (dark blue region)' with a higher number of conformations less than median G-scale (dark to light blue region) which reduced to two clusters (dark blue region) for RpsE-Spectinomycin complex (Fig. 8a). The overall change (RMSD) in the final protein conformation with respect to the parent structure was 3.30 Å, 4.64 Å and 7.30 Å for RpsE-Lead_1, RpsE-Lead_2 and RpsE-Spectinomycin complex respectively, which implied a greater conformational change in the RpsE while complexed with the antibiotic than the proposed leads.

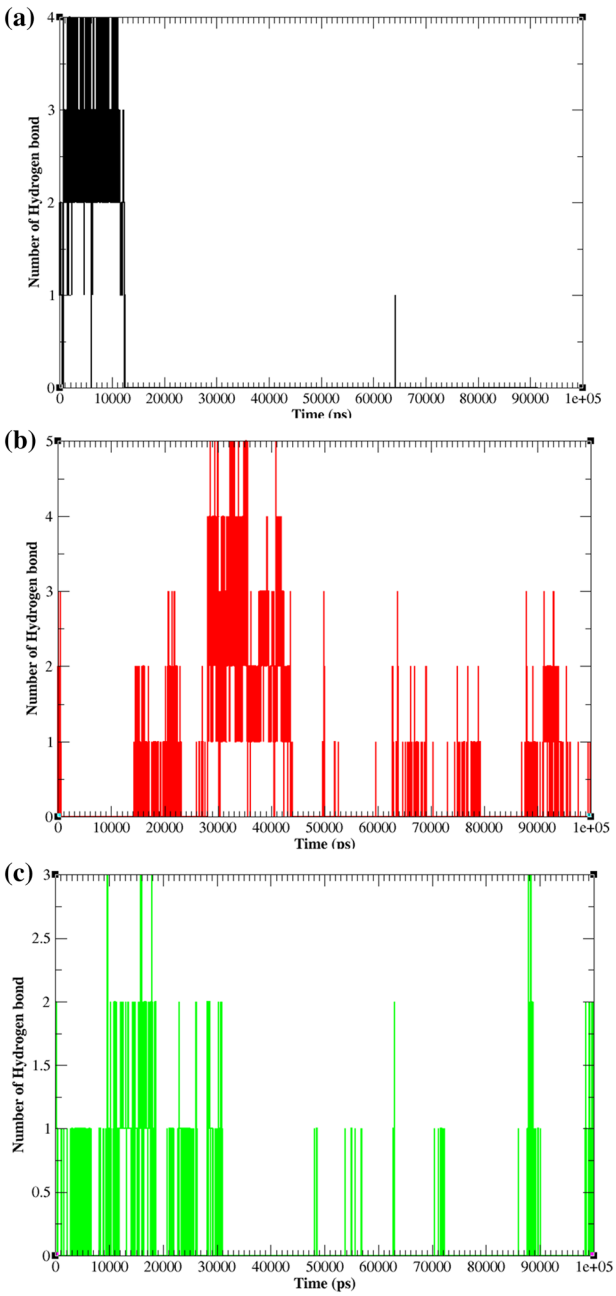

Fig. 7 Hydrogen bonding profiles of RpsE-lead molecules complexes as compared to RpsE-spectinomycin complex in the timeframe of 100 ns: **a** number of hydrogen bonds in RpsE-spectinomycin complex, **b** number of hydrogen bonds in RpsE-Lead_1 complex, **c** number of hydrogen bonds in RpsE-Lead_2 complex

DISCUSSION

The present study investigated alternative treatment strategies against MDR *E. cloacae* ATCC 13047 by employing GIN approach and structural bioinformatics methods. Interaction network study of the AMR genes revealed clustering patterns (Fig. 1a) based on the functional associations of the genes. The three clusters, although each comprised genes belonging to different functional categories, were highly interconnected. Cluster C1 genes encoded for Ribosomal, RNA polymerase, DNA gyrase and DNA topoisomerase IV subunit proteins (Fig. 1b), out of which certain ribosomal subunit proteins aided in *Helicobacter pylori* cell survival under oxidative stress; however they have not been conventionally explored as therapeutic drug targets (Sun et al. 2012). On the other hand, the absence of any direct interaction between *gyrA* and *parC* as well as in *gyrB* and *parE*, all being fluoroquinolone-resistance determining genes (PF03989; IPR013757; SM00434), implied that the genes worked independently, but their functions towards

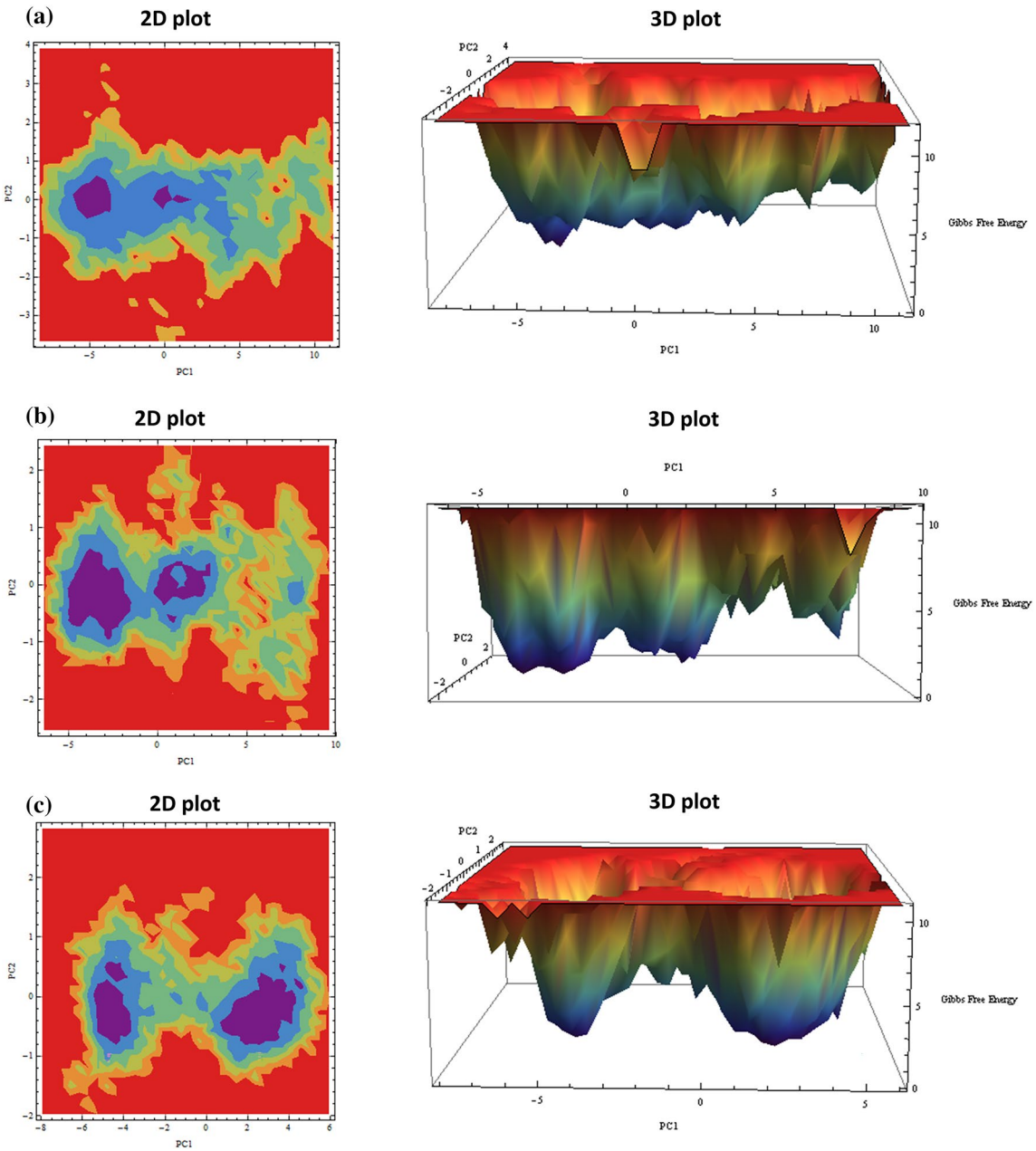

Fig. 8 Principal component analysis (PCA) and free energy landscape (FEL): the FEL contour plots displayed as a function of PC1 and PC2, whose cosine content values were less than 0.2 were shown as 2D contour and 3D distribution plot. Using 2D- and 3D-FEL plots, two PCs (PC1 and PC2) of **a** RpsE-spectinomycin; **b** RpsE-Lead_1 and **c** RpsE-Lead_2 complexes were projected. RpsE-Lead_1 and RpsE-Lead_2 complexes showed three distinct 'lowest free energy cluster basins (dark blue region)' with a higher number of conformations less than median G-scale (dark to light blue region) which reduced to two clusters (dark blue region) for RpsE-Spectinomycin complex

quinolone resistance remain conjoined. Rather than targeting GyrA, B and ParC, E proteins exhibiting frequent mutations in active sites (Rafii et al. 2005), proteins required for general metabolic processes and having direct associations with AMR proteins could be instead considered as alternative therapeutic markers that can hinder bacterial survival under stress (Sharma et al. 2019). Hence, from C1 cluster it was inferred that the inactivation of 30S ribosomal protein S5 (RpsE) could lead to possible interference in the translation of vital proteins involved in bacterial physiology, drug resistance and survival under stress. Cluster C2 genes were predominantly involved in AMR efflux pump mechanisms-ABC transport superfamily (MacB, MsbA) and RND superfamily (AcrA,B, OqxA,B, MdtC) (Fig. 1b). The

cluster further highlighted *macB*, *acrA* and *acrB* as highly interacting genes, which have also been previously proposed as therapeutic targets against AMR-linked bacterial infections (Miryala et al. 2021a; Debroy and Ramaiah 2022). Furthermore, experimental reports have implied resistance patterns by *acrA,B* towards β-lactams and CAMP molecules in *Salmonella typhimurium* and *E. coli* respectively (Nikaido et al. 1998), thus correlating with the FEA of *acrA,B* from the current study (ecln01501; ecln01503). Interaction profile and FEA indicated AcrA as the interlinking molecule of the C2 cluster, which can be a potential hub protein candidate. Cluster C3 cluster comprised of *arn* genes predominantly involved in CAMP resistance (Fig. 1b), which function by imparting modification in the lipid A moiety of Lipopolysaccharides, lowering the net negative charge of membrane and reducing its binding affinity with CAMP molecules (Lin et al. 2014). In C3, *arnT*, associated with polymyxin resistance, was noted as the interlinking biomolecule among the other *arn* genes and hence can be a potent hub gene for subduing CAMP resistance. Thus from the overall clustering analysis and FEA, three potential drug target candidates were shortlisted, namely, 30S ribosomal subunit S5 (RpsE) (cytoplasmic), AcrA (inner cell membrane) and ArnT (inner cell membrane), and are yet to be exploited sufficiently as therapeutic targets in the strain. All three proteins are coded by chromosomal genes, implying that the drug resistance imparted by these AMR genes is inherent for the organism, which may result in the exhibition of opportunistic characteristics by the bacteria (Barker 1999). The three therapeutic drug targets were screened out bypassing the proteins responding under oxidative stress and the MDR proteins reporting repeated mutations in the emerging strains which pose a dilemma in targeting them. Hence, the drug targets discussed in the current study were alternative in terms of treatment and held novelty in the strain. Topological matrices-based screening further highlighted RpsE to be selected as a potential drug target in the organism (Supplementary File S3).

S5 is a small subunit ribosomal protein linked to the functional center of the 30S ribosomal subunit and can regulate translational fidelity if structurally altered (Kirthi et al. 2006). RpsE protein in *E. cloacae* consists of RNA binding domain lying towards the *N*-terminal of the protein, within which 23rd, 26th, 29th, 30th and 32nd amino acid residues were observed to be highly conserved across prokaryotic and archaebacterial organisms in the previous studies (Ramakrishnan and White 1992). Reports have suggested that a single amino acid mutation in *E. coli* S5 can result in spectinomycin-resistance, other than alteration of cell growth and folding of 16S ribosomal RNA (Kirthi et al. 2006). Conservation of its tertiary structure was reported to be evident throughout the genetic evolution, which correlated with backbone dynamics analysis in the present study (Fig. 3f) revealing less dynamicity of the RNA-binding domain backbone, possibly attributing towards uniform functionality of the protein domain (Basu et al. 2021; Debroy and Ramaiah 2022). The rigid backbone of the RNA-binding region can be required to accommodate a larger substrate like nucleic acid, carbohydrate, etc., rather than requiring a relatively flexible backbone to make transient bonds with smaller substrates like ATP. A meager peak observed in the RMSF plot within 22nd–33rd amino acid residues (Fig. 4b) might be reasoned for potential flexibility in the region (as previously noted in the backbone stability plot as well) resulting in possible transient intermolecular interactions with small molecules or ions; however, reports have suggested high mutational frequencies at around 20th–22nd amino acid residues in *E. coli* owing to spectinomycin resistance (Ramakrishnan and White 1992). On the other hand, the commercially available compounds, namely ZINC5441082 (*N*-Isopentyladenosine) (Lead_1) and ZINC1319816 (Cyclopentyl-aminopurinyl-hydroxymethyl-oxolanediol) (Lead_2) were predicted to be oral drug-candidates against RpsE protein. The proposed lead compounds are nucleoside analogues with similar known targets. *N*-Isopentyladenosine [PubChem CID: 87216] has been checked against targets such as adenosine kinases, adenosine transporters, Histone-lysine *N*-methyltransferases (epigenetic regulator) and cytokinin oxidases. On the other hand, Cyclopentyl-aminopurinyl-hydroxymethyloxolanediol [PubChem CID: 14426724] has been tested against human Histone-lysine *N*-methyltransferases, Tyrosine-protein kinases, adenosine kinases and cytosolic proteins Glyceraldehyde-3-phosphate dehydrogenases.

Previous studies have documented the affinity of Spectinomycin and its derivatives against aminoglycoside modifying enzymes (AMEs) that mediate aminoglycoside-resistance. Higher affinity to AMEs ($\Delta G < -5.0$ kcal/mol) results in the preferential binding of AMEs to the antibiotics, hindering their potency from binding with the desired targets (Ioana et al. 2016). Similarly, the comparative affinity of Spectinomycin and closely related drugs were evaluated using *in silico* docking methods showing moderate affinity against various targets from reference (susceptible) *Enterobacter* strains (Zhou et al. 2018). Sufficient *in silico-in vitro* combination studies have validated the emerging resistance to aminoglycosides (e.g. Spectinomycin) in *Enterobacter* sp. (Katsu et al. 1982). *In silico* studies have previously explored ribosomal proteins as drug targets for therapeutic interventions (Miryala et al. 2021b; Basu et al. 2022a). Ribosomal proteins targeting conventional antibiotics derivatives have been explored to exhibit multi-target affinity in bacterial and viral pathogens. Previous studies have shown the prospect of targeting RpsE, since it is devoid of dominant resistance-conferring mutations in *Enterobacter* sp. Hence, our study intended to address the limitation of therapeutics through computational drug repurposing against the rarely

exploited RpsE as a drug target. In the present study, molecular docking results showed that Lead_1 (by 0.8 kcal/mol and 0.66 mM) and Lead_2 (by 0.02 kcal/mol and 0.3 mM) required less energy to bind with RpsE and lower concentration to inhibit RNA-binding activity of RpsE as compared to its standard antibiotic Spectinomycin (Dharuman et al. 2021). However, higher number of conventional H-bonds and fewer non-canonical interactions were noted in RpsE_Spectinomycin complex compared to the other two complexes (Fig. 5). This could be validated from the binding free energy (G_{bind}) calculations indicating lower linear interaction energy for RpsE_Spectinomycin complex (~ − 200 kJ/mol) than RpsE-Lead_1 (~ − 100 kJ/mol) and RpsE-Lead_2 (~ − 100 kJ/mol) (Fig. 6g). In contrast, less number of stable H-bonds in RpsE_Spectinomycin (four H-bonds) in the time-frame of 100 ns was noted than in RpsE-Lead_1 complex (five H-bonds) in the H-bond profile (Fig. 7). The PCA-based FEL graphs were plotted using the top two PCs to gain a better understanding of the plausible state of protein structures along with their corresponding Gibbs free energy. Due to the higher number of low energy clusters for RpsE-Lead_1 and RpsE-Lead_2 complexes, there is a higher probability of transient bond formations between protein and ligand molecules, thus favoring an increased chance of targeting RpsE (Fig. 8). While the FEL plot of RpsE_Spectinomycin complex indicated fewer regions of low energy clusters implying chemical inertness of RpsE protein while binding to the antibiotic, thus reducing the chance of inhibition. The results have hence supported the hypothesis that the proposed nucleoside analogues Lead_1 and Lead_2 can efficiently bind to the functional domain of RpsE and can result in fruitful inhibition of the protein activity. The above findings have been generated through Knowledge-guided computational therapeutic predictions. However, the research work could not lead to *in-vitro* validations. However, our findings will be a good starting point for experimental validations and can be taken up as a future extension of the study.

CONCLUSION

To conclude, the current study focused on the GIN approach to study the interconnecting and functional hub genes from MDR *E. cloacae* ATCC 13047 in order to identify the potential drug target for subsequent structural assessment. From the GIN, topological and FEA revealed *rpsE*, *acrA* and *arnT* as potential drug targets from C1, C2 and C3 clusters respectively. Targeting their respective expressed products can impart detrimental impacts on the survival machinery of *E. cloacae* ATCC 13047. RpsE, attaining the highest topological scores out of the three proposed therapeutic drug targets, was selected for extensive structural evaluation and stability profile. Ligand-based virtual screening, pharmacokinetic and ADME screening predicted ZINC5441082 (*N*-Isopentyladenosine) (Lead_1) and ZINC1319816 (cyclopentyl-aminopurinyl-hydroxymethyl-oxolanediol) (Lead_2) as novel lead molecules against RpsE. Molecular docking and MDS studies indicated the binding efficiency and structural stability of the protein−ligand complexes, which was further supported by binding free energy calculations, PCA and FEL analyses. Hence, the predicted commercially available nucleoside analogues and their specific therapeutic drug target, RpsE, can be exploited for designing new antibacterial compounds.

Supplementary information The online version contains supplementary material available at https://doi.org/10.1007/s11274-023-03634-z.

Acknowledgements The authors gratefully acknowledge the Indian Council of Medical Research (ICMR), Government of India agency, for the research grant (IRIS ID: 2020-0690). The authors would like to thank the management of VIT for providing the necessary facilities to carry out the research work. The authors would like to sincerely thank Prof. (Dr.) Anand Anbarasu, VIT-Vellore, for his invaluable intellectual suggestions and perpetual support throughout the research work. The authors would like to thank Mr. Soumya Basu (Teaching cum Research Assistant—VIT, Vellore) and Mr. Aniket Naha (Scientist—Pushpagiri Institute of Medical Sciences and Research Centre, Tiruvalla) for their expert inputs in molecular dynamics simulations. The authors would also like to thank Dr. Manikandan Jayaraman (Research Scientist—Alagappa University, Karaikudi) for his expert inputs in PCA based FEL analysis. RD would like to thank ICMR for her Senior Research fellowship (Project ID: 2021-10632).

Author contributions RD: Data collection, analysis and manuscript writing. SR: Study conceptualization, funding requisition, supervision, final review.

Funding The authors gratefully acknowledge the Indian Council of Medical Research (ICMR), Government of India agency, for the research grant (IRIS ID: 2020-0690).

Data availability All the data generated or analyzed during this study are included in this research article (and its supplementary files).

Declarations

Competing interest The authors declare no competing interests.

Ethics approval The present research did not involve the use of human or animal subjects.

References

Alam K, Islam MM, Islam S et al (2023) Comparative genomics with evolutionary lineage in *Streptomyces* bacteria reveals high biosynthetic potentials. World J Microbiol Biotechnol 39:64. https://doi.org/10.1007/s11274-022-03433-y

Ashok G, Ramaiah S (2022) A critical review of datasets and computational suites for improving cancer theranostics and biomarker discovery. Med Oncol 39:206. https://doi.org/10.1007/s12032-022-01815-8

Ashok G, Miryala SK, Anbarasu A, Ramaiah S (2021) Integrated systems biology approach using gene network analysis to identify the important pathways and new potential drug targets for neuroblastoma. Gene Rep 23:101101. https://doi.org/10.1016/j.genrep.2021.101101

Ashok G, Miryala SK, Saju MT et al (2022) FN1 encoding fibronectin as a pivotal signaling gene for therapeutic intervention against pancreatic cancer. Mol Genet Genom 297:1565–1580. https://doi.org/10.1007/s00438-022-01943-w

Bader GD, Hogue CW (2003) An automated method for findingmolecular complexes in large protein interaction networks. Nucleic Acids Res 29:137–140. https://doi.org/10.1093/nar/29.1.137

Barker KF (1999) Antibiotic resistance: a current perspective. Br J Clin Pharmacol 48:109–124. https://doi.org/10.1046/j.1365-2125.1999.00997.x

Basu S, Naha A, Veeraraghavan B et al (2021) In silico structure evaluation of BAG3 and elucidating its association with bacterial infections through protein–protein and host-pathogen interaction analysis. J Cell Biochem https://doi.org/10.1002/jcb.29953

Basu S, Debroy R, Kumar H et al (2022a) Bioactive phytocompounds against specific target proteins of *Borrelia recurrentis* responsible for louse-borne relapsing fever: genomics and structural bioinformatics evidence. Med Vet Entomol. https://doi.org/10.1111/mve.12623

Basu S, Varghese R, Debroy R, et al (2022b) Non-steroidal anti-inflammatory drugs ketorolac and etodolac can augment the treatment against pneumococcal meningitis by targeting penicillin-binding proteins. Microb Pathog 170:105694. https://doi.org/10.1016/j.micpath.2022.105694

Bollen A, Davies J, Ozaki M, Mizushima S (1969) Ribosomal protein conferring sensitivity to the antibiotic Spectinomycin in *Escherichia coli*. Science 165:85–86. https://doi.org/10.1126/science.165.3888.85

Choudhary P, Waseem M, Kumar S et al (2023) Y12F mutation in *Pseudomonas plecoglossicida* S7 lipase enhances its thermal and pH stability for industrial applications: a combination of in silico and in vitro study. World J Microbiol Biotechnol 39:75. https://doi.org/10.1007/s11274-023-03518-2

Cilia E, Pancsa R, Tompa P et al (2014) The dynamine webserver: predicting protein dynamics from sequence. Nucleic Acids Res 42:264–270. https://doi.org/10.1093/nar/gku270

Daina A, Michielin O, Zoete V (2017) SwissADME—a free web tool to evaluate pharmacokinetics, drug-likeness and medicinal chemistry friendliness of small molecules. Sci Rep 7:42717. https://doi.org/10.1038/srep42717

Debroy R, Ramaiah S (2022) MurC ligase of multi-drug resistant *Salmonella typhi* can be inhibited by novel curcumin derivative: evidence from molecular docking and dynamics simulations. Int J Biochem Cell Biol 151:106279. https://doi.org/10.1016/j.biocel.2022.106279

Dey J, Mahapatra SR, Lata S et al (2022a) Exploring *Klebsiella pneumoniae* capsule polysaccharide proteins to design multiepitope subunit vaccine to fight against pneumonia. Expert Rev Vaccines 21:569–587. https://doi.org/10.1080/14760584.2022.2021882

Dey J, Mahapatra SR, Patnaik S et al (2022b) Molecular characterization and designing of a novel multiepitope vaccine construct against *Pseudomonas aeruginosa*. Int J Pept Res Ther 28:49. https://doi.org/10.1007/s10989-021-10356-z

Dey J, Mahapatra SR, Raj TK et al (2022c) Designing a novel multiepitope vaccine to evoke a robust immune response against pathogenic multidrug-resistant *Enterococcus faecium* bacterium. Gut Pathog 14:21. https://doi.org/10.1186/s13099-022-00495-z

Dharuman S, Wilt LA, Liu J et al (2021) Synthesis, antibacterial action, and ribosome inhibition of deoxyspectinomycins. J Antibiot (Tokyo) 74:381–396. https://doi.org/10.1038/s41429-021-00408-3

Eugene Sanders WE, Sanders CC (1997) *Enterobacter* spp.: pathogens poised to flourish at the turn of the century. Clin Microbiol Rev 10:220–241. https://doi.org/10.1128/cmr.10.2.220

Fiannaca A, La Rosa M, Urso A, et al (2013) A knowledge-based decision support system in bioinformatics: an application to protein complex extraction. BMC Bioinformatics 14:S5. https://doi.org/10.1186/1471-2105-14-S1-S5

Gasteiger E, Hoogland C, Gattiker A et al (2005) Protein identification and analysis tools on the expasy server. Proteom Protoc Handb. https://doi.org/10.1385/1-59259-890-0:571

Geourjon C, Deléage G (1995) Sopma: significant improvements in protein secondary structure prediction by consensus prediction from multiple alignments. Bioinformatics 11:681–684. https://doi.org/10.1093/bioinformatics/11.6.681

Godara A, Kao KC (2020) Adaptive laboratory evolution for growth coupled microbial production. World J Microbiol Biotechnol 36:175. https://doi.org/10.1007/s11274-020-02946-8

Hamelberg D, Mongan J, McCammon JA (2004) Accelerated molecular dynamics: a promising and efficient simulation method for biomolecules. J Chem Phys 120:11919–11929. https://doi.org/10.1063/1.1755656

Hanwell MD, Curtis DE, Lonie DC, et al (2012) Avogadro: an advanced semantic chemical editor, visualization, and analysis platform. J Cheminform 4:1–17. https://doi.org/10.1186/1758-2946-4-17

He X, Miao V, Baltz RH (2005) Spectinomycin Resistance in rpsE mutants is recessive in *Streptomyces roseosporus*. J Antibiot (Tokyo) 58:284–288. https://doi.org/10.1038/ja.2005.35

Heo L, Park H, Seok C (2013) Galaxyrefine: protein structure refinement driven by side-chain repacking. Nucleic Acids Res 41:384–388. https://doi.org/10.1093/nar/gkt458

Ioana I, Dan Cristian V, Ilioara O, et al (2016) Biological evaluation and molecular docking of some chromenyl derivatives as potential antimicrobial agents. Pak J Pharm Sci 29:261–272

Jayaraman M, Rajendra SK, Ramadas K (2019) Structural insight into conformational dynamics of non-active site mutations in kasa: a *Mycobacterium tuberculosis* target protein. Gene 720:144082. https://doi.org/10.1016/j.gene.2019.144082

Jayaraman M, Loganathan L, Muthusamy K, Ramadas K (2021) Virtual screening assisted discovery of novel natural products to inhibit the catalytic mechanism of *Mycobacterium tuberculosis* inhA. J Mol Liq 335:116204. https://doi.org/10.1016/j.molliq.2021.116204

Kaplan W, Littlejohn TG (2001) Swiss-PDB viewer (deep view). Brief Bioinform 2:195–197. https://doi.org/10.1093/bib/2.2.195

Katsu K, Inoue M, Mitsuhashi S (1982) Transposition of the carbenicillin-hydrolyzing beta-lactamase gene. J Bacteriol 150:483–489. https://doi.org/10.1128/jb.150.2.483-489.1982

Kaviraj M, Kumar U, Nayak AK, Chatterjee S (2022) Homology modeling and virtual characterization of cytochrome c nitrite reductase (NrfA) in three model bacteria responsible for short-circuit pathway, DNRA in the terrestrial nitrogen cycle. World J Microbiol Biotechnol 38:168. https://doi.org/10.1007/s11274-022-03352-y

Kim DE, Chivian D, Baker D (2004) Protein structure prediction and analysis using the Robetta server. Nucleic Acids Res 32:W526–W531. https://doi.org/10.1093/nar/gkh468

Kirthi N, Roy-Chaudhuri B, Kelley T, Culver GM (2006) A novel single amino acid change in small subunit ribosomal protein S5 has profound effects on translational fidelity. RNA 12:2080–2091. https://doi.org/10.1261/rna.302006

Kumar R, Jayaraman M, Ramadas K, Chandrasekaran A (2020) Insight into the structural and functional analysis of the impact of missense mutation on cytochrome P450 oxidoreductase. J Mol Graph Model 100:107708. https://doi.org/10.1016/j.jmgm.2020.107708

Lemkul J (2019) From proteins to perturbed Hamiltonians: a suite of tutorials for the GROMACS-2018 molecular simulation package

[Article v1.0]. Living J Comput Mol Sci 1:1–53. https://doi.org/10.33011/livecoms.1.1.5068

Lin QY, Tsai YL, Liu MC et al (2014) *Serratia marcescens* arn, a PhoP-regulated locus necessary for polymyxin B resistance. Antimicrob Agents Chemother 58:5181–5190. https://doi.org/10.1128/AAC.00013-14

Mahapatra SR, Dey J, Jaiswal A et al (2022a) Immunoinformatics-guided designing of epitope-based subunit vaccine from pilus assembly protein of *Acinetobacter baumannii* bacteria. J Immunol Methods 508:113325. https://doi.org/10.1016/j.jim.2022.113325

Mahapatra SR, Dey J, Raj TK et al (2022b) The potential of plant-derived secondary metabolites as novel drug candidates against *Klebsiella pneumoniae*: molecular docking and simulation investigation. S Afr J Bot 149:789–797. https://doi.org/10.1016/j.sajb.2022.04.043

McGuffin LJ, Bryson K, Jones DT (2000) The PSIPRED protein structure prediction server. Bioinformatics 16:404–405. https://doi.org/10.1093/bioinformatics/16.4.404

Miryala SK, Anbarasu A, Ramaiah S (2021a) Gene interaction network to unravel the role of gut bacterial species in cardiovascular diseases: E. coli O157:H7 host-bacterial interaction study. Comput Biol Med 133:104417. https://doi.org/10.1016/j.compbiomed.2021.104417

Miryala SK, Basu S, Naha A et al (2021b) Identification of bioactive natural compounds as efficient inhibitors against *Mycobacterium tuberculosis* protein-targets: a molecular docking and molecular dynamics simulation study. J Mol Liq 341:117340. https://doi.org/10.1016/j.molliq.2021.117340

Naha A, Ramaiah S (2022) Structural chemistry and molecular-level interactome reveals histidine kinase EvgS to subvert both antimicrobial resistance and virulence in *Shigella flexneri* 2a str. 301. 3 Biotech 12:258. https://doi.org/10.1007/s13205-022-03325-w

Naha A, Vijayakumar S, Lal B et al (2021) Genome sequencing and molecular characterisation of XDR *Acinetobacter baumannii* reveal complexities in resistance: novel combination of sulbactam–durlobactam holds promise for therapeutic intervention. J Cell Biochem 122:1946–1957. https://doi.org/10.1002/jcb.30156

Naha A, Banerjee S, Debroy R, et al (2022) Network metrics, structural dynamics and density functional theory calculations identified a novel ursodeoxycholic acid derivative against therapeutic target parkin for Parkinson's disease. Comput Struct Biotechnol J 20:4271–4287. https://doi.org/10.1016/j.csbj.2022.08.017

Narang PK, Dey J, Mahapatra SR et al (2021) Functional annotation and sequence-structure characterization of a hypothetical protein putatively involved in carotenoid biosynthesis in microalgae. S Afr J Bot 141:219–226. https://doi.org/10.1016/j.sajb.2021.04.014

Narang PK, Dey J, Mahapatra SR, et al (2022) Genome-based identification and comparative analysis of enzymes for carotenoid biosynthesis in microalgae. World J Microbiol Biotechnol 38:8. https://doi.org/10.1007/s11274-021-03188-y

Nikaido H, Basina M, Nguyen V, Rosenberg EY (1998) Multidrug efflux pump AcrAB of *Salmonella typhimurium* excretes only those β-lactam antibiotics containing lipophilic side chains. J Bacteriol 180:4686–4692. https://doi.org/10.1128/jb.180.17.4686-4692.1998

Pettersen EF, Goddard TD, Huang CC et al (2004) UCSF chimera—a visualization system for exploratory research and analysis. J Comput Chem 25:1605–1612. https://doi.org/10.1002/jcc.20084

Priyamvada P, Debroy R, Anbarasu A, Ramaiah S (2022) A comprehensive review on genomics, systems biology and structural biology approaches for combating antimicrobial resistance in ESKAPE pathogens: computational tools and recent advancements. World J Microbiol Biotechnol. https://doi.org/10.1007/s11274-022-03343-z

Pugalenthi G, Shameer K, Srinivasan N, Sowdhamini R (2006) HARMONY: a server for the assessment of protein structures. Nucleic Acids Res 34:W231–W234. https://doi.org/10.1093/nar/gkl314

Rafii F, Park M, Novak JS (2005) Alterations in DNA gyrase and topoisomerase IV in resistant mutants of *Clostridium perfringens* found after in vitro treatment with fluoroquinolones. Antimicrob Agents Chemother 49:488–492. https://doi.org/10.1128/AAC.49.2.488-492.2005

Ramakrishnan V, White SW (1992) The structure of ribosomal protein S5 reveals sites of interaction with 16S rRNA. Nature 358:768–771. https://doi.org/10.1038/358768a0

Ren Y, Ren Y, Zhou Z et al (2010) Complete genome sequence of *Enterobacter cloacae* subsp. cloacae type strain ATCC 13047. J Bacteriol 192:2463–2464. https://doi.org/10.1128/JB.00067-10

Rifai EA, van Dijk M, Vermeulen NPE et al (2019) A comparative linear interaction energy and MM/PBSA study on SIRT1-ligand binding free energy calculation. J Chem Inf Model 59:4018–4033. https://doi.org/10.1021/acs.jcim.9b00609

Sahoo P, Dey J, Mahapatra SR et al (2022) Nanotechnology and COVID-19 convergence: toward new planetary health interventions against the pandemic. Omi A J Integr Biol 26:473–488. https://doi.org/10.1089/omi.2022.0072

Shankar C, Basu S, Lal B et al (2021) Aerobactin seems to be a promising marker compared with unstable RmpA2 for the identification of hypervirulent carbapenem-resistant *Klebsiella pneumoniae*: in silico and in vitro evidence. Front Cell Infect Microbiol. https://doi.org/10.3389/fcimb.2021.709681

Shannon P, Markiel A, Owen Ozier 2, et al (2003) Cytoscape: a software environment for integrated models of biomolecular interaction networks. Genome Res 13:2498–2504. https://doi.org/10.1101/gr.1239303.metabolite

Sharma P, Garg N, Sharma A, et al (2019) Nucleases of bacterial pathogens as virulence factors, therapeutic targets and diagnostic markers. Int J Med Microbiol 309:151354. https://doi.org/10.1016/j.ijmm.2019.151354

Sharma A, Sanduja P, Anand A, et al (2021) Advanced strategies for development of vaccines against human bacterial pathogens. World J Microbiol Biotechnol 37:67. https://doi.org/10.1007/s11274-021-03021-6

Sinha R, Sharma B, Dangi AK, Shukla P (2019) Recent metabolomics and gene editing approaches for synthesis of microbial secondary metabolites for drug discovery and development. World J Microbiol Biotechnol 35:166. https://doi.org/10.1007/s11274-019-2746-2

Sudeshna Panda S, Dey J, Mahapatra SR et al (2022) Investigation on structural prediction of pectate lyase enzymes from different microbes and comparative docking studies with pectin: the economical waste from food industry. Geomicrobiol J 39:294–305. https://doi.org/10.1080/01490451.2021.1992042

Sun Y, Li X, Li W et al (2012) Proteomic analysis of the function of spot in *Helicobacter pylori* anti-oxidative stress in vitro and colonization in vivo. J Cell Biochem 113:3393–3402. https://doi.org/10.1002/jcb.24215

Swargiary A, Mahmud S, Saleh MA (2020) Screening of phytochemicals as potent inhibitor of 3-chymotrypsin and papain-like proteases of SARS-CoV2: an in silico approach to combat COVID-19. J Biomol Struct Dyn 0:1–15. https://doi.org/10.1080/07391102.2020.1835729

Swetha RG, Ramaiah S, Anbarasu A (2017) R521C and R521H mutations in FUS result in weak binding with karyopherinβ2 leading to amyotrophic lateral sclerosis: a molecular docking and dynamics study. J Biomol Struct Dyn 35:2169–2185. https://doi.org/10.1080/07391102.2016.1209130

Szklarczyk D, Morris JH, Cook H, et al (2017) The STRING database in 2017: quality-controlled protein–protein association networks,

made broadly accessible. Nucleic Acids Res 45:D362–D368. https://doi.org/10.1093/nar/gkw937

Trivedi MK, Harish Shettigar SP (2015) In vitro evaluation of biofield treatment on *Enterobacter cloacae*: impact on antimicrobial susceptibility and biotype. J Bacteriol Parasitol 06:0–6. https://doi.org/10.4172/2155-9597.1000241

Varghese R, Basu S, Neeravi A et al (2022) Emergence of meropenem resistance among cefotaxime non-susceptible *Streptococcus pneumoniae*: evidence and challenges. Front Microbiol 12:4111. https://doi.org/10.3389/fmicb.2021.810414

Vasudevan K, Basu S, Arumugam A et al (2021) Identification of potential carboxylic acid-containing drug candidate to design novel competitive NDM inhibitors: an in-silico approach comprising combined virtual screening and molecular dynamics simulation. Res Prepr. https://doi.org/10.1101/2021.07.05.451101

Volkamer A, Kuhn D, Rippmann F, Rarey M (2012) Dogsitescorer: a web server for automatic binding site prediction, analysis and druggability assessment. Bioinformatics 28:2074–2075. https://doi.org/10.1093/bioinformatics/bts310

von Mering C (2003) STRING: a database of predicted functional associations between proteins. Nucleic Acids Res 31:258–261. https://doi.org/10.1093/nar/gkg034

Wang S, Li W, Liu S, Xu J (2016) Raptorx-property: a web server for protein structure property prediction. Nucleic Acids Res 44:W430–W435. https://doi.org/10.1093/nar/gkw306

Wattam AR, Abraham D, Dalay O et al (2014) PATRIC, the bacterial bioinformatics database and analysis resource. Nucleic Acids Res 42:581–591. https://doi.org/10.1093/nar/gkt1099

Webb B, Sali A (2017) Protein structure modeling with MODELLER. Methods Mol Biol 1654:39–54. https://doi.org/10.1007/978-1-4939-7231-9_4

Wiederstein M, Sippl MJ (2007) ProSA-web: interactive web service for the recognition of errors in three-dimensional structures of proteins. Nucleic Acids Res 35:407–410. https://doi.org/10.1093/nar/gkm290

Yang J, Zhang Y (2015) I-TASSER server: new development for protein structure and function predictions. Nucleic Acids Res 43:W174–W181. https://doi.org/10.1093/nar/gkv342

Zhou K, Yu W, Cao X et al (2018) Characterization of the population structure, drug resistance mechanisms and plasmids of the community-associated *Enterobacter cloacae* complex in China. J Antimicrob Chemother 73:66–76. https://doi.org/10.1093/jac/dkx361

Zoete V, Daina A, Bovigny C, Michielin O (2016) SwissSimilarity: a web tool for low to ultra high-throughput ligand-based virtual screening. J Chem Inf Model 56:1399–1404. https://doi.org/10.1021/acs.jcim.6b00174